Revision 1

Incorporation of Y and REEs in aluminosilicate garnet: Energetics from atomistic simulation

WILLIAM D. CARLSON[1,*], JULIAN D. GALE[2], KATE WRIGHT[2]

[1]Department of Geological Sciences, University of Texas at Austin, 2275 Speedway Stop C9000, Austin Texas 78712 USA

[2] Nanochemistry Research Institute, Department of Chemistry, Curtin University, GPO Box U1987, Perth WA 6845, Australia

*Email: wcarlson@jsg.utexas.edu

Running title: Incorporation of Y and REEs in garnet

Always consult and cite the final, published document. See http://www.minsocam.org or GeoscienceWorld

20

Always consult and cite the final, published document. See http://www.minsocam.org or GeoscienceWorld

Incorporation of Y and REEs in aluminosilicate garnet: Energetics from atomistic simulation

ABSTRACT

Yttrium and the rare-earth elements (Y+REEs) are incorporated into aluminosilicate garnet as trivalent ions replacing divalent Mg, Fe, Mn, or Ca ("M^{2+}") in dodecahedral sites, which requires some form of coupled substitution to maintain electroneutrality. We compare the energetic costs of competing coupled-substitution schemes, using lattice dynamics calculations to assess defect energies and exchange energies for each scheme. Substitutions with relatively low energetic costs introduce menzerite-like components via the exchange vector $[YM_{-1}\cdot(Mg,Fe)Al_{-1}]$, or alkali components via the exchange vector $[Y(Na,Li)M_{-2}]$. Substitutions with substantially higher energetic costs introduce a vacancy component via the exchange vector $[Y_2\square M_{-3}]$, or the yttrogarnet (YAG) component via the exchange vector $[YM_{-1}\cdot AlSi_{-1}]$, or a component with octahedral Li via the exchange vector $[Y_2M_{-2}\cdot LiAl_{-1}]$. Energetic costs decrease significantly as the host-garnet unit-cell dimension expands, decrease very modestly as temperature rises or pressure falls, and decrease substantially with the contraction in ionic radius across the lanthanide series. These results, combined with critical re-examination of arguments cited in favor of each substitution scheme in natural occurrences, suggest that Y+REE incorporation in natural garnet is dominated by coupled substitutions that introduce menzerite and alkali components, that the YAG substitution plays only a subsidiary role, and that the other schemes are likely to be of very minor importance.

Keywords: garnet, yttrium, rare-earth elements, lattice dynamics, atomistic simulation

Always consult and cite the final, published document. See http://www.minsocam.org or GeoscienceWorld

INTRODUCTION

The crystallochemical means by which yttrium and the rare-earth elements (Y+REEs) are incorporated into aluminosilicate garnet in Earth's crust and upper mantle are not definitively known, even though these elements' concentrations and zoning in garnet have considerable importance to diverse petrological and geochronological processes and systems.

The geological significance of Y+REEs in garnet takes many forms. A classic example is the control exerted by garnet-liquid partitioning on the REE concentrations of mantle melts sourced from garnet peridotite (e.g., Hanson 1980; van Westrenen and Draper 2007; Sun and Liang 2013). In the deep crust, zoning of Y+REEs in metamorphic garnet is a sensitive monitor of the processes that enhance or inhibit equilibration between garnet and the mineral assemblage and/or fluid environment in which it grows (Skora et al. 2006; Konrad-Schmolke et al. 2008; Moore et al. 2013). Valuable thermometers arise from equilibrium Y partitioning between garnet and monazite (Pyle et al. 2001) and between garnet and xenotime (Pyle and Spear 2000). In favorable cases, Y+REE zoning in garnet records the evolution of coexisting accessory minerals (such as allanite, monazite, xenotime and zircon) vital to geochronometry of successive assemblages (e.g., Pyle and Spear 1999; Pyle et al. 2001; Yang and Rivers 2002; Hermann and Rubatto 2003; Yang and Pattison 2006; Gieré et al. 2011). The characteristic partitioning of REEs between garnet and zircon can link zircon U-Pb ages to garnetiferous mineral assemblages suitable for thermobarometry, adding detail and precision to *P-T-t* paths (e.g., Rubatto 2002). REE incorporation is of course the fundamental basis for Sm-Nd and Lu-Hf geochronology of garnet (cf. Kohn 2009). The diffusional mobility of Y+REEs in garnet, with its attendant implications for the kinetics of petrologic processes (e.g., Van Orman et al. 2002; Tirone et al.

Always consult and cite the final, published document. See http://www.minsocam.org or GeoscienceWorld

2005) and for geochronology (e.g, Kohn 2009; Kelly et al. 2011), depends directly upon the means by which local electroneutrality is maintained as these atoms move through the garnet structure (Carlson 2012).

Despite the varied and important roles played by Y+REEs in garnet, the question of how these large trivalent ions are accommodated in the garnet structure remains unanswered. Although several potential substitutional schemes have been proposed, their relative importance in nature is unclear, and for some, even their validity is uncertain. If and how these schemes may be affected by temperature and pressure is also poorly known. To address some of these issues, this study uses atomistic simulation, in the form of lattice dynamics, to evaluate the comparative energetic costs of introducing each of the proposed substitutional defects into otherwise unmodified garnet structures, across a range of temperature and pressure.

BACKGROUND

This investigation is focused on large trivalent ions (Y+REEs), those whose ionic radii exceed the size that allows ready substitution into the sites normally occupied by Al in aluminosilicate garnet. Unlike smaller trivalent cations (e.g., Fe^{3+}, Cr^{3+}, V^{3+}) that can replace Al via simple homovalent substitution in octahedral sites, Y+REEs must enter the larger dodecahedral sites, normally occupied by divalent cations, via more complex heterovalent substitutions that require coupled exchanges to maintain charge balance.

Typically, Y is by far the most abundant large-radius trivalent ion found in natural garnet: its concentration is commonly a factor of 10-100 greater than those of the heavy rare-earth elements (HREEs), and a factor of 100-1000 greater than those of the light rare-earth elements (LREEs). Consequently, the focus of most experimental and analytical studies of heterovalent

Always consult and cite the final, published document. See http://www.minsocam.org or GeoscienceWorld

91 substitution schemes for these ions has been on Y. We adopt a similar focus in this study, but
92 also examine in reconnaissance the effects of variations in ionic size across the lanthanide series.

93 **Garnet structure and crystal chemistry**

94 Natural aluminosilicate garnet crystallizes in space group $Ia\bar{3}d$ (Menzer 1928) with
95 compositions close to $M_3Al_2Si_3O_{12}$, in which M represents one or more of the four divalent
96 cations that dominate in garnet solid-solutions in Earth's lower crust and upper mantle: Mg, Fe,
97 Mn, and Ca, in end-members pyrope (Pyp), almandine (Alm), spessartine (Sps), and grossular
98 (Grs), respectively. Unit-cell dimensions scale with the size of the M cation; at ~298 K and 1 bar,
99 a_0 (Prp) = 1.1457 nm; a_0 (Alm) = 1.1525 nm; a_0 (Sps) = 1.1614 nm; and a_0 (Grs) = 1.1852 nm
100 (Ganguly et al. 1993; Geiger and Feenstra 1997).

101 In terms of coordination by oxygen atoms, M sites are eightfold (triangular dodecahedral),
102 Al sites are sixfold (octahedral), and Si sites are fourfold (tetrahedral); all polyhedra are distorted
103 from regularity to varying degrees. Connectivity among polyhedra is extensive and complex (cf.
104 Bosenick et al. 2000), producing chains of continuous edge-sharing dodecahedra, of alternating
105 edge-sharing dodecahedra and octahedra, of alternating edge-sharing dodecahedra and
106 tetrahedra, and of alternating corner-sharing octahedra and tetrahedra (Fig. 1).

107 As noted above, the large size of Y+REE ions—1.019 Å for $^{VIII}Y^{3+}$, and ranging from
108 1.143 Å for $^{VIII}Ce^{3+}$ to 0.977 Å for $^{VIII}Lu^{3+}$ (Shannon 1976)—dictates that these trivalent cations
109 must occupy the dodecahedral sites, which normally house divalent cations. Their incorporation
110 therefore requires some form of charge compensation, which leads to a variety of possible
111 coupled-substitution schemes that maintain electroneutrality.

112 **Proposed substitution schemes for Y incorporation**

Always consult and cite the final, published document. See http://www.minsocam.org or GeoscienceWorld

In the prior literature, four types of coupled substitutions have been invoked as ways to preserve local charge balance when making the heterovalent exchange of trivalent Y (or REE) for a divalent cation in a dodecahedral site. These substitution schemes are described below, along with a fifth scheme that has not been considered in detail previously. Figure 1 depicts graphically the site occupancies produced by each of the coupled substitutions.

YAG. The exchange vector [$YM_{-1}{\cdot}AlSi_{-1}$] maintains charge balance by incorporating a "yttrogarnet" or YAG component $Y_3Al_2Al_3O_{12}$, replacing tetrahedral Si with Al. This substitution scheme was proposed by Jaffe (1951), who noted the similarity in ionic radii of Y^{3+} and Mn^{2+} and the "frequent association of yttrium and manganese in spessartites" (p. 131), and hypothesized the incorporation of tetrahedral Al for charge balance. Yoder and Keith (1951) synthesized the end-member yttrogarnet (now commonly termed "YAG", for yttrium-aluminum garnet) as part of a solution series with spessartine, confirming the feasibility of Jaffe's proposed substitution scheme. Since that time, the YAG component (occasionally together with its iron analog YIG = $Y_3Fe^{3+}{}_2Fe^{3+}{}_3O_{12}$) has commonly been assumed to be a principal means of Y incorporation in natural garnet (e.g., Kasowski and Hogarth 1968; the Fe3+-garnet group of Enami et al. 1995; Pyle et al. 2001; Røhr et al. 2007; van Westrenen and Draper 2007; and many others).

^{VIII}VACANCY ($^{VIII}\square$). The exchange vector [$Y_2\square M_{-3}$] maintains charge balance by incorporating a vacancy component $Y_2\square Al_2Si_3O_{12}$, leaving one dodecahedral site unoccupied for each two Y atoms that are introduced. For the REEs, Bea et al. (1997) adopted this substitution scheme as their explanation for measured trace-level concentrations of REE^{3+} ions that they interpreted as reflecting more extensive incorporation at higher pressures. They regarded the YAG substitution as an unsatisfactory alternative, hypothesizing that it should lead to

Always consult and cite the final, published document. See http://www.minsocam.org or GeoscienceWorld

enlargement of the unit cell and thus reduce Y+REE incorporation at higher pressures. Noting "the lack of positive correlation between MREE [*middle REEs*] with any other trace element with a suitable ionic radius able to compensate that of the MREE ions through a coupled substitution" (p. 266), they favored the vacancy exchange, arguing that it would reduce the size of the unit cell, and thus be favored by increases in pressure.

Quartieri et al. (1999b) attempted a test for the operation of this substitution scheme by measuring Yb L_I-edge and Yb L_{III}-edge XANES spectra for synthetic pyrope and grossular containing ~1 wt. % Yb. For grossular, theoretical model spectra were calculated for different local environments around Yb, and they observed (p. 93) that the model spectra placing vacancies adjacent to Yb^{2+} "are more similar to those of the experimental spectra", leading them to state: "Notwithstanding that these qualitative observations cannot be considered as conclusive, they support the hypothesis that charge balance occurs through a substitution mechanism involving vacant X[*dodecahedral*]-sites."

Van Orman et al. (2002, p. 420) later invoked this vacancy substitution scheme in explanation of their experimental observation that REE diffusion rates at trace levels in natural pyrope had little or no dependence on ionic radius.

^{VIII}ALKALI (^{VIII}NA or ^{VIII}LI). The exchange vector [$YNaM_{-2}$] maintains charge balance by incorporating the alkali component $Y_{1.5}Na_{1.5}Al_2Si_3O_{12}$, introducing $^{VIII}Na^+$ in place of an M^{2+} ion. Initial recognition of this substitution scheme is attributed to Semenov (1963; not seen: reported by Kasowski and Hogarth 1968, p. 556, and by Grew et al. 2010, p. 1191). It was invoked by Enami et al. (1995) to explain compositions of orthogneiss-hosted Ca- and Mn-rich aluminosilicate garnet containing up to 0.37 wt. % Na_2O, 2.1 wt. % Y_2O_3, and 0.48 wt. % Yb_2O_3, in which the atomic ratio Na/(Y+Yb) is close to unity (0.79-1.19) and in which Na and (Y+Yb)

Always consult and cite the final, published document. See http://www.minsocam.org or GeoscienceWorld

co-vary in zoned crystals. In contrast, they reported that in related occurrences, garnet rich in andradite component (And; $Ca_3Fe^{3+}{}_2Si_3O_{12}$) has much lower Na/(Y+Yb) (0.17-0.18), and yields slightly sub-silicic EPMA analyses, which they regarded as indications that a YAG component is the predominant means of Y incorporation in these crystals. Small Na/(Y+Yb) ratios in aluminosilicate garnet from a lower pressure pegmatite, in comparison with the above large ratios in aluminosilicate garnet from the higher pressure orthogneiss, led to the conclusion that the ^{VIII}NA substitution is favored over the YAG substitution at elevated pressures. Using similar reasoning for crystals of comparable trace-element compositions, Røhr et al. (2007) likewise inferred the operation of both YAG and ^{VIII}NA substitutions, with the latter favored at higher pressure.

The equivalent lithium exchange vector [$YLiM_{-2}$] maintains charge balance by incorporating the component $Y_{1.5}Li_{1.5}Al_2Si_3O_{12}$, introducing $^{VIII}Li^+$ in place of the divalent M^{2+} ion. Cahalan et al. (2012, in review) offered this substitution as the most likely explanation for coupled diffusion of Y and Li in partially resorbed natural garnets.

Menzerite (MNZ-MG or MNZ-FE). The exchange vectors [$YM_{-1}{\cdot}MgAl_{-1}$] and [$YM_{-1}{\cdot}FeAl_{-1}$] maintain charge balance by incorporating menzerite-type components $Y_2MMg_2Si_3O_{12}$ and $Y_2MFe_2Si_3O_{12}$, replacing octahedral Al with either Mg or Fe. These substitution schemes were described by Grew et al. (2010), who identified a new natural garnet species, menzerite-(Y), in which all other Y (+REE) components were shown to be much lower in abundance than $Y_2Ca(Mg,Fe)_2Si_3O_{12}$. The basis for this claim was a comprehensive investigation combining optical microscopy, single-crystal X-ray diffractometry, synchrotron X-ray absorption spectroscopy, and electron-probe microanalysis.

Always consult and cite the final, published document. See http://www.minsocam.org or GeoscienceWorld

Carlson's (2012) analysis of diffusion rates for Y+REE in garnet led to the inference that menzerite substitutions predominate over other modes of Y+REE incorporation in natural deep-crustal garnets. Because these substitutions require that the exchange of Y+REE for dodecahedral M cations must be linked directly to the exchange of Mg and/or Fe for octahedral Al ions, they provide a straightforward explanation for several otherwise enigmatic aspects of Y+REE diffusivity — namely, the weak dependence of diffusivity on ionic radius and host-garnet composition, the near-equivalence of the diffusivities of Y+REEs with that of Cr, and the strong positive cross-coupling among simultaneously diffusing Y+REEs.

^{VI}Li. The exchange vector [$Y_2M_{-2}{\cdot}LiAl_{-1}$] maintains charge balance by incorporating a lithium component $Y_2MLiAlSi_3O_{12}$, introducing ^{VI}Li in place of Al. This substitution scheme has not been previously described in detail, but by analogy to the MNZ-MG and MNZ-FE substitutions, its viability is suggested by the fact that the ionic radius (Shannon 1976) of ^{VI}Li (0.76 Å) falls between those of ^{VI}Mg (0.72 Å) and ^{VI}Fe (0.78 Å). Hanrahan et al. (2009) touch upon the possibility that Li incorporation in garnet at $P < 6$ GPa involves octahedrally coordinated Li, although no mention is made of how electroneutrality would be preserved. Cahalan et al. (in review) included this ^{VI}LI substitution scheme as a potential, but less likely, alternative to the ^{VIII}LI substitution scheme for coupling the diffusion of Li and Y.

PREVIOUS WORK

This investigation of Y+REE incorporation in garnet employs atomistic simulation in the form of lattice dynamics calculations. Similar approaches have been taken—with distinctly different goals—in several previous studies of garnet energetics and thermodynamics, as introduced briefly here.

Always consult and cite the final, published document. See http://www.minsocam.org or GeoscienceWorld

In their study of element-partitioning between garnet and silicate melts, van Westrenen et al. (2000) investigated a wide range of both homovalent and heterovalent substitutions in aluminosilicate garnet (Pyp, Alm, Sps, and Grs), including a suite of REEs incorporated by means of YAG-type and ^{VIII}ALKALI-type substitution schemes. In the static limit (T = 0 K, P = 0 GPa), they computed: (a) the "relaxation energy", that is, the strain energy released upon adjustment of the structure to its minimum-energy configuration after introduction of a defect into an unrelaxed structure; and (b) the "solution energy", that is, the energy of exchange of substituent elements between garnet and coexisting sources/sinks in a melt, as approximated by solid binary oxides. These results succeeded in rationalizing trends in experimental observations that related garnet/melt partitioning to substituent charge and radius.

Bosenick et al. (2000), focusing on the pyrope-grossular join, examined the local structural response to Ca/Mg substitution and the energetics of dodecahedral ordering of Ca and Mg in solid solutions along the join. Their lattice dynamics calculations in the static limit demonstrated that strain effects govern the energetics of dodecahedral Ca/Mg substitution, leading to short-range ordering of Ca and Mg. These results were combined with Monte Carlo simulations to evaluate the corresponding NMR cluster occupancy, ordering energy, and configurational entropy of the short-range ordering process.

Becker and Pollok (2002) evaluated interfacial and thermodynamic mixing properties of garnet compositions along the grossular-andradite join. Relaxed lattice energies for random configurations of solutions with different Fe:Al ratios yielded cation-cation interaction parameters, which were then used in Monte Carlo simulations to obtain thermodynamic properties. The calculations predicted the stability of an ordered 1:1 structure at T < ~500 K and low-T miscibility gaps between the end-members and intermediate solution compositions.

Always consult and cite the final, published document. See http://www.minsocam.org or GeoscienceWorld

A series of investigations by van Westrenen and others (van Westrenen et al. 2003a, b; Freeman et al. 2005; Freeman et al. 2006) explored in detail the effects of short range ordering in solid solutions along the pyrope-grossular join, focusing on local cation environments in the static limit, and employing both classical and first-principles approaches. These calculations demonstrated that a key factor for the energetics of the solid solution, and also for the incorporation of impurities, was the size of cations occupying pairs of dodecahedra that share edges with a common bridging tetrahedron: energy minimization requires avoidance or removal of high-strain Mg-Mg pairs that distort the shared Si tetrahedron. In parallel with these studies, Lavrentiev et al. (2006) examined both the pyrope-grossular and the pyrope-almandine solid solutions at 0-2000K and 0-15 GPa, obtaining thermodynamic mixing properties. They computed near-ideal behavior for the pyrope-almandine join but strongly non-ideal behavior for the pyrope-grossular join, and confirmed the high energetic cost of incorporating Mg-Si-Mg cation groups in this solid solution even at elevated temperatures and pressures.

Vinograd et al. (2004) combined static lattice energy calculations with the cluster expansion formalism to predict pairwise interactions along the pyrope-grossular join, then used the Cluster Variation Method to obtain activity-composition relations. The results confirmed that the size mismatch between Ca and Mg produces short-range ordering, and a miscibility gap was predicted to appear below 500 °C.

Vinograd et al. (2006) also evaluated the pyrope-majorite join in a similar fashion, again starting with static lattice energy calculations, but then using the cluster expansion model to obtain temperature-dependent properties through Monte Carlo simulation; free energies of mixing and ordering were retrieved by thermodynamic integration of the Monte Carlo results. Activity-composition relationships along the join were determined, conditions for the cubic-

Always consult and cite the final, published document. See http://www.minsocam.org or GeoscienceWorld

tetragonal transition in majorite were computed, and a miscibility gap associated with the transition was identified.

ATOMISTIC SIMULATION OF DEFECT ENERGIES IN GARNET

Our use of atomistic simulation to investigate Y+REE incorporation in garnet is driven by the recognition that analytical determination of the substitutional schemes that operate in nature is rarely definitive. Conclusive results have come only for the ^{VIII}NA and MNZ substitutions (e.g., Enami et al. 1995; Grew et al. 2010), in analyses of unusual occurrences in which Y+REE components comprise several wt. % of the garnet, rather than the levels of tens to hundreds of ppm that occur most commonly. Insights into other proposed substitutional schemes, particularly in more dilute natural systems, must be sought by other means.

A key consideration is the energy required to introduce, as defects in an otherwise pristine crystal structure, an Y or REE ion and its charge-compensating counterpart: all else being equal, lower-energy schemes should be favored in nature over their higher-energy alternatives. The energetic costs of various defects can be evaluated and compared by atomistic simulation. In our case, a lattice dynamics calculation is performed in which a force-field is defined to describe the interactions among ions in the structure, and the defect energy is computed as the difference between the lattice energy of the pristine structure and that of the structure relaxed to its minimum-energy configuration after introduction of the substituent ions.

Potentials

All of our interatomic potentials are based on an ionic model, using formal integral charges. Short-range cation-oxygen and oxygen-oxygen interactions employ two-body Buckingham potentials, in which the interatomic potential U between ions separated by distance r is given by $U(r) = A \cdot \exp(-r/\rho) - (C/r^6)$. Cation-cation interactions, beyond electrostatics, are

Always consult and cite the final, published document. See http://www.minsocam.org or GeoscienceWorld

neglected because Coulomb repulsion is usually sufficient. Oxygen-ion polarizability is included via the shell model of Dick and Overhauser (1958), in which the core-shell interaction potential at separation r is given by $U(r) = ½\ k\ r^2$. A three-body O–Si–O bending term is included, in which the potential due to deviation from an ideal bond angle θ_0 is given by $U(\theta) = ½\ K_B\ (\theta - \theta_0)^2$. To maximize consistency with the prior literature, we used the potentials employed by van Westrenen et al. (2000), modifying their Li^+–O^{2-} parameters (see below) and adding the Y^{3+}–O^{2-} potential of Lewis and Catlow (1985). These potentials have seen widespread and successful application in prior mineralogical investigations; their parameters and the original sources for those values are compiled in Table 1.

We also considered the set of potentials employed by Bosenick et al. (2000). Although they used the same Si^{4+}–O^{2-} potential as van Westrenen et al. (2000), they chose a different Al^{3+}–O^{2-} potential that included a three-body bending term, and also made a concerted effort to evaluate multiple possible potentials for Mg^{2+}–O^{2-} and Ca^{2+}–O^{2-}. Their intent was to reproduce specific, compositionally dependent distortions of polyhedra in the pyrope and grossular structures that were particularly important to their aims. For Mg^{2+}–O^{2-}, their evaluation led them to select the same potential used by Van Westrenen et al.; but for Ca^{2+}–O^{2-}, they employed a different potential, which, despite yielding an undesirably small unit-cell dimension and short Al–O bond lengths in grossular, was characterized as giving "in total the best, albeit least bad, model for grossular" (p. 404). Bosenick et al. did not evaluate the Ca^{2+}–O^{2-}potential used by Van Westrenen et al.

The potential set—and in particular the Ca^{2+}–O^{2-}potential—used by Bosenick et al. is, however, apparently ill-suited to the goals of the present study. As seen in Table 2, those potentials underestimate the cell dimension of grossular, such that its bulk and shear moduli are

Always consult and cite the final, published document. See http://www.minsocam.org or GeoscienceWorld

exceptionally high in comparison to experimental measurements. In terms of defect energies, this is manifested in values for grossular that rise anomalously above trends *vs.* cell dimension that are otherwise well-defined by calculations for pyrope, almandine and spessartine. The potential set that we prefer yields a unit-cell dimension for grossular that is only marginally better, but its relative errors for elastic moduli of grossular are two to four times smaller than those produced by the potential set used by Bosenick et al.; our choice also yields smooth trends for defect energies *vs.* cell dimension across the range of garnet end-member compositions.

New parameters for the Li^{+}–O^{2-} potential were derived for this study, following the discovery that the potential used by Van Westrenen et al. yields a structure for Li_2O that includes a dynamical instability in the form of an imaginary phonon frequency for the zone boundary transverse acoustic mode along the [110] direction. This problem was rectified by a fit of the Li^{+}–O^{2-} potential parameters to the Li_2O structure that included as a constraint the experimental value for this frequency (Farley et al. 1988), along with the cell dimension and elastic constants. The new potential parameters appear in Table 1.

Procedures

GULP, the General Utility Lattice Program (Gale 1997; Gale and Rohl 2003), was used for all simulations. To investigate possible variations in the relative energies of substitution schemes as functions of temperature and pressure, defect energies were evaluated over a range of *T-P* conditions: 1000, 1200, and 1400 K, each at 1, 2, and 3 GPa.

Defect energies were obtained by comparing the Gibbs free energy of a pristine garnet structure to the Gibbs free energy of the same structure following ionic substitution and relaxation to the state at which net forces on all atoms are equal to zero. For each garnet end-member, a 2x2x2 supercell with composition $M_{192}Al_{128}Si_{192}O_{768}$ was generated, and its structure

Always consult and cite the final, published document. See http://www.minsocam.org or GeoscienceWorld

at each desired combination of temperature and pressure was optimized via free energy minimization. Free energy minimization utilized the formalism introduced by Kantorovich (1995), as implemented by Gale (1998), employing the zero static internal stress approximation (ZSISA) (Allan et al. 1996) to conform to the quasiharmonic approximation. The resultant structure was then modified by a single unit of substitutional exchange along a selected vector, relaxed at constant volume, and its free energy re-evaluated at the chosen temperature and pressure. We note that formally the use of a constant-volume calculation means that the Helmholtz, rather than Gibbs, free energy is derived. However, given that the bulk structure is relaxed at constant pressure prior to creation of the defect, these two free energies become equivalent at infinite dilution (Taylor et al. 1997).

In similar fashion, the Gibbs free energies of the binary oxides involved in exchange reactions were determined by optimizing a single unit cell at each desired combination of temperature and pressure via free energy minimization under ZSISA.

ENERGIES OF DEFECTS AND SUBSTITUTIONAL EXCHANGES

Evaluating the relative energies of Y+REE incorporation via different substitution schemes requires consideration not only of the stoichiometry of the exchanges, but also of the lattice free energies of the materials that serve as sources and sinks for the inserted and removed ions, and of the specific configuration (relative structural positions) of the ions involved. Here we describe our choice for reference sources and sinks, and our approach to identification of the minimum-energy configurations for each of the defects.

Exchange reactions

Y+REE incorporation into garnet is a substitutional exchange, for which the total energetic cost depends not only on the energy of the defect in garnet, but also upon the pre- or post-

Always consult and cite the final, published document. See http://www.minsocam.org or GeoscienceWorld

341 substitution energies of the ions that are inserted into or removed from garnet when the defect is
342 created. Any selected set of sources and sinks for exchanged ions constitutes a reference state for
343 the substitution energies. The choice of reference state has no effect on the relative energies of
344 various configurations for a particular defect. However, the values of the exchange energies—
345 and thus comparisons within and across host compositions—will vary from one reference state to
346 another. In nature, the sources and sinks for the interchanged ions are the coexisting minerals
347 that approach or achieve exchange equilibrium with garnet. The energetics of Y+REE
348 incorporation in garnet therefore depend explicitly upon the mineral assemblage, but vary only to
349 the extent that the local atomic environments of the exchanged ions differ among possible sets of
350 coexisting minerals.

351 Our computations used simple binary oxides as the sources and sinks for the interchanged
352 ions. This approach is equivalent to assuming that the energy of the local atomic environment for
353 an exchanged ion in its oxide is equivalent to the energy of that environment in whatever
354 minerals equilibrate with garnet in a natural mineral assemblage. For example, consider Mg as
355 the ion removed from garnet when an Y ion is introduced, and MgO as the sink for that ion. This
356 substitution transfers the Mg ion into a site with octahedral coordination by oxygen, a local
357 atomic environment that is very similar to the Mg site in most minerals that might serve as Mg
358 sinks in nature (e.g., olivine in peridotite, perhaps orthopyroxene in granulite). The use of binary
359 oxides to define reference states is a widely employed approach. It has proved valuable even for
360 garnet-melt partitioning studies, in which local atomic environments in binary oxides were
361 successfully used to approximate environments in a silicate melt that serves as the source and
362 sink for exchanged ions (van Westrenen et al. 2000; van Westrenen et al. 2003b).

Always consult and cite the final, published document. See http://www.minsocam.org or GeoscienceWorld

Table 3 lists the reactions used to compute the free energies of Y incorporation in aluminosilicate garnet; the difference in free energy between products and reactants for each reaction is the *exchange energy* ΔG_{xch}. As an example, consider the exchange reaction for the YAG substitution

$$M_3Al_2Si_3O_{12} + ½\ Y_2O_3 + ½\ Al_2O_3 = YM_2{\cdot}Al_2{\cdot}AlSi_2{\cdot}O_{12} + MO + SiO_2$$

for which the exchange energy is given by

$$\Delta G_{xch} = [G(YM_2{\cdot}Al_2{\cdot}AlSi_2{\cdot}O_{12}) + G(MO) + G(SiO_2)] - [G(M_3Al_2Si_3O_{12}) + ½\ G(Y_2O_3) + ½\ G(Al_2O_3)]$$

$$= [G(YM_2{\cdot}Al_2{\cdot}AlSi_2{\cdot}O_{12}) - G(M_3Al_2Si_3O_{12})] + G(MO) + G(SiO_2) - ½\ G(Y_2O_3) - ½\ G(Al_2O_3)\ .$$

The bracketed quantity in the final expression above is the *defect energy* ΔG_{def}, evaluated by the supercell approach. The last four terms are lattice free energies for the binary oxides; their computed values are compiled in Table 4. At all conditions, lattice free energies of binary oxides were computed for the structures stable at 298K and 1 bar, ignoring any phase changes that would preferentially stabilize alternative polymorphs at elevated temperature and pressure; thus, for example, the α-quartz structure was used for SiO_2 under all conditions.

We note in passing that if information on exchange energies for a particular mineral assemblage is desired, an equivalent approach could be taken that simply modifies the exchange reactions to include the specific minerals in the assemblage in place of the binary oxides. An appreciation for the approximate magnitude of these effects of variations in mineral assemblage comes from a small set of exploratory calculations, in which Mg and Fe components of olivine and orthopyroxene were used as the sources for Mg and Fe in exchange reactions for the MNZ-MG and MNZ-FE substitutions. For the MNZ-MG substitution, the difference in exchange energy for Mg sourced from an olivine-bearing assemblage vs. an orthopyroxene-bearing assemblage is 51 $kJ{\cdot}mol^{-1}$; for the MNZ-FE substitution, the difference is 50 $kJ{\cdot}mol^{-1}$. (These differences are, of

Always consult and cite the final, published document. See http://www.minsocam.org or GeoscienceWorld

386 course, the same for all host-garnet compositions.) It therefore seems reasonable to assume that
387 in natural occurrences, variations in mineral assemblages in diverse bulk compositions will
388 perturb absolute exchange energies by several tens of $kJ \cdot mol^{-1}$.

389 **Defect energies in minimum-energy configurations**

390 The proximity of each substituent atom to its charge-compensating counterpart(s) affects
391 the value of the defect energy: some configurations have lower defect energies than others, and
392 they should therefore be favored. A common premise (cf. Purton et al. 1997, p. 3930; van
393 Westrenen et al. 2000, p. 1631) is that the lowest-energy configuration results when the
394 substituent atoms are as close to one another as possible. We identified the minimum-energy
395 configuration for each of the seven Y-in-garnet defects by calculating and comparing defect
396 energies in a systematic variety of configurations at 1200 K and 2 GPa; full details appear in
397 Appendix 1 (Depository item AM-YEAR-XXX)[1].

398 For all two-atom substitutional schemes—YAG, ^{VIII}NA or ^{VIII}LI, and MNZ-MG or MNZ-FE—the
399 lowest-energy configuration is indeed a nearest-neighbor arrangement minimizing the distance
400 between the charge-compensating ions (Fig. 1). For YAG, the Al atom enters a tetrahedron that
401 shares an edge with the Y-bearing dodecahedron, rather than one that shares a corner. For ^{VIII}NA
402 or ^{VIII}LI, the alkali atom enters one of the four dodecahedra immediately adjacent to the Y-
403 bearing dodecahedron, all of which are symmetrically equivalent. For MNZ-MG or MNZ-FE, the
404 divalent cation enters an octahedron immediately adjacent to the Y-bearing dodecahedron.

405 The remaining substitutional schemes require replacement of three atoms, inserting two
406 Y^{3+} ions together with either $^{VIII}\square$ or $^{VI}Li^{+}$. Systematic sampling of the large number of possible

[1] Deposit item AM-YEAR-XXX, Appendix 1. Deposit items are available two ways: For a paper copy contact the Business Office of the Mineralogical Society of America (see inside front cover of recent issue) for price information. For an electronic copy visit the MSA web site at http://www.minsocam.org, go to the American Mineralogist Contents, find the table of contents for the specific volume/issue wanted, and then click on the deposit link there.

Always consult and cite the final, published document. See http://www.minsocam.org or GeoscienceWorld

configurations identified, for each scheme, two similar configurations whose energies differ by < 3 kJ·mol^{-1} (see Appendix 1); the configuration with the (negligibly) lower energy in almandine was selected. For these two-Y substitution schemes, each minimum-energy configuration (Fig. 1) can be rationalized as one that optimizes the trade-offs involved in simultaneously maximizing the Y-Y distance, minimizing the Y-(□,Li) distances for both Y ions, and avoiding excessive polyhedral distortions. For ^{VIII}□, the two Y-bearing dodecahedra share opposite edges of the vacant dodecahedron. For ^{VI}Li, two Y-bearing dodecahedra that both share edges with the Li-bearing octahedron can adopt three configurations that produce different Y-Y distances. In the minimum-energy configuration, the Y-bearing dodecahedra do not share edges with one another (which would minimize the Y-Y distance), and do not lie on opposite sides of the octahedron (which would maximize the Y-Y distance), but instead are configured to yield an intermediate Y-Y distance.

Defect energies for coupled substitutions adopting these minimum-energy configurations are presented in Table 5, and all subsequent calculations and comparisons are based upon these configurations.

Defect energies calculated via the supercell approach will include interactions among neighboring defects, if these interactions extend over distances greater than the spacing of defects in the supercell. A good approximation of the magnitudes of these interactions is obtained by comparing internal energies calculated in the static limit (T = 0, P = 0) for defects in the supercell with those calculated for isolated defects using an embedded-cluster method and the two-region Mott-Littleton procedure (Mott and Littleton 1938). This comparison was made for all seven defect types in each of the four compositional end members. Internal energies of the periodic defects in 2x2x2 supercells were larger by 1-4 kJ·mol^{-1} than internal energies of

Always consult and cite the final, published document. See http://www.minsocam.org or GeoscienceWorld

individual isolated defects. The strongest interactions arose among ^{VIII}NA and ^{VIII}LI defects (3-4 kJ·mol^{-1}); MNZ-MG, MNZ-FE, and ^{VI}LI interactions yielded intermediate values (2-3 kJ·mol^{-1}); and the weakest interactions were calculated for YAG and ^{VIII}□ defects (1-2 kJ·mol^{-1}).

The effects of defect interactions in the simulations should be similar to those in nature. A single Y atom in a 2x2x2 supercell corresponds to an Y concentration of ~3000 ppm, which falls comfortably within the range of natural Y+REE concentrations for garnet—roughly a few hundred ppm to perhaps 2-3 wt. %—although in nature the defect distribution is not likely to be strictly periodic.

Energies of substitutional exchanges

Table 6 presents the calculated exchange energies for each of the proposed Y substitutional schemes in each of the four end-member aluminosilicate garnets, at temperatures of 1000, 1200 and 1400 K and pressures of 1, 2, and 3 GPa. The effect on exchange energies of host-garnet composition is illustrated in Figure 2, using example data at 1200 K and 2 GPa. Although the exchange energies in Table 6 also show appreciable thermal and barometric variation, these effects are due primarily to changes in the lattice energies of the binary oxides used to define the reference state for the substitutional energies, with the defect energies themselves playing only a subsidiary role. This is made evident in Figures 3 and 4, which plot the defect energies directly, isolating the energetic effects within garnet from other influences. Figure 3 shows the effects of temperature at 2 GPa, and Figure 4 shows the effects of pressure at 1200 K; both use data for almandine as an example. All substitutional schemes exhibit slight increases in defect energy at higher pressure, and all but ^{VIII}□ show slight reductions in defect energy at higher temperature (defect energies for ^{VIII}□ increase slightly with temperature). The central finding, however, is that

Always consult and cite the final, published document. See http://www.minsocam.org or GeoscienceWorld

all of these effects of temperature and pressure are quite small, at most a few tens of $kJ \cdot mol^{-1}$ across the full range of conditions illustrated.

Differences in ionic radii across the lanthanide series will influence defect energies for REE incorporation. We explored this effect by computing defect energies and evaluating exchange energies in almandine for selected lanthanides (La, Nd, Eu, Gd, Ho, Yb and Lu) at 1200 K and 2 GPa. The exchange energies are reported in Table 7, and Figure 5 illustrates their variation with ionic radius.

DISCUSSION

In natural occurrences, lower-energy schemes for Y+REE incorporation should predominate over higher-energy schemes. But as described above, the energetics of Y+REE incorporation into garnet cannot be evaluated precisely without taking into account the energy transfers involved in exchanging ions between garnet and the minerals that serve as sources and sinks for the elements involved in the substitutions. The examples above comparing olivine-bearing assemblages to orthopyroxene-bearing assemblages as sources and sinks for Fe and Mg suggest that such variations might perturb exchange energies by several tens of $kJ \cdot mol^{-1}$. We focus now on the energy differences identified in this study that are very much larger than this, and that are therefore are likely to be robust with respect to the range of natural variability in sources and sinks for substituent elements.

Relative importance of substitutional schemes in natural garnets

In the following, we interpret our calculations as evidence that the YAG, $^{VIII}\square$, and ^{VI}LI substitution schemes are energetically so costly that they will account for only a minor fraction of the Y+REE found in natural garnet. Conversely, the MNZ and ^{VIII}ALKALI substitution schemes,

Always consult and cite the final, published document. See http://www.minsocam.org or GeoscienceWorld

as the energetically least costly means of Y+REE incorporation, are much more likely to account for the commonly observed uptake of these elements.

Energetically unfavorable substitution schemes: YAG, $^{VIII}\square$, and ^{VI}LI. Figure 2 illustrates that in all host compositions, defects based on the YAG and $^{VIII}\square$ substitution schemes have much higher exchange energies than their alternatives, which implies that they are far less likely to occur in nature. The same is mostly true for the ^{VI}LI substitution scheme, although in grossular its energetic cost is comparable to that of the ^{VIII}ALKALI schemes. As described above, however, both YAG and $^{VIII}\square$ have enjoyed substantial popularity in the literature, which prompts the following critical re-assessment of the evidence for them.

The apparent basis for assigning Y incorporation in natural garnets to a YAG substitution is the successful crystallization by Yoder and Keith (1951) of several members of a solid-solution series between spessartine and yttrogarnet in the experimental system $3MnO{\cdot}Al_2O_3{\cdot}3SiO_2$ – $3Y_2O_3{\cdot}5Al_2O_3$. Jaffe (1951, p. 148) quite reasonably regarded the experimental synthesis results as confirmation of his inference that the YAG substitution operated in his natural Mn-rich and Y-rich garnets, but he did so without evidence for the presence of tetrahedral Al. Subsequent studies that invoke the YAG substitution in nature appear to rely on the precedent of Jaffe. None of them documents directly the existence of ^{IV}Al in the structure to provide charge balance for Y, which is of course a difficult task; instead, most simply regard the YAG substitution as the fallback explanation when the Na/(Y+REE) ratio is insufficient to account for all Y+REE incorporation by means of the ^{VIII}Na scheme (Enami et al. 1995, p. 480; Røhr et al. 2007, p. 1282). In some instances, the presence of ^{IV}Al is inferred from apparently sub-silicic EPMA analyses, for which Si concentrations are calculated to be < 3 apfu, based on 8-cation or 12-oxygen renormalization (Enami et al. 1995, p. 480; Røhr et al. 2007, Table 1). But a rigorous

Always consult and cite the final, published document. See http://www.minsocam.org or GeoscienceWorld

497 justification for assignment of small amounts of Al to tetrahedral sites in garnet, based solely on
498 EPMA data, requires an analytical protocol capable of unusually high accuracy, especially in the
499 absence of independent determinations of H content, of F content, and of the Fe^{2+}/Fe^{3+} and
500 Mn^{2+}/Mn^{3+} ratios. It should of course be noted that all of these studies predated the discovery of
501 menzerite-(Y) as a new mineral species, so none of them considered the MNZ-MG or MNZ-FE
502 substitutions as possibilities.

503 Arguments favoring a $^{VIII}\square$ substitution scheme are offered by Bea et al. (1997) and
504 Quartieri et al. (1999b). Bea et al.'s inference is indirect, and is intended to explain a rise in trace
505 REE concentrations in natural garnet with increasing pressure. Presuming that the only
506 alternative to the YAG substitution is the $^{VIII}\square$ substitution (that is, without taking into account the
507 ^{VIII}ALKALI and MNZ substitutions), they reasoned that $^{VIII}\square$, unlike YAG, would reduce the molar
508 volume of the garnet structure and therefore be favored by increasing pressure. As seen in
509 Figures 2 and 4, however, our calculations of the exchange energies and defect energies reveal
510 that the $^{VIII}\square$ substitution is very substantially higher in energetic cost than the YAG substitution
511 at all pressures, and in fact the $^{VIII}\square$ defect energy increases with pressure at a rate twice as large
512 as the rate of increase for the YAG defect. It seems clear that either different substitutional
513 schemes are responsible for their measured rise in REE concentrations with pressure, or perhaps
514 the presumed basis for the increase in REE contents is not pressure, but one of the other factors
515 the authors considered but dismissed (p. 264), namely temperature, bulk-garnet composition, or
516 whole-rock composition—and changing stability of REE-bearing accessory minerals is a further
517 possibility worthy of consideration. Quartieri et al. (1999b) worked on pure synthetic end-
518 member pyrope and grossular, doped with ~1 wt. % Yb_2O_3. In these compositionally restricted
519 experimental systems, available substitutions are limited, and in the case of grossular, the YAG

Always consult and cite the final, published document. See http://www.minsocam.org or GeoscienceWorld

and $^{VIII}\square$ substitution schemes would be the only ones possible. For grossular, they calculated theoretical model spectra for three cases: one in which all four dodecahedral sites surrounding a central Yb^{3+} ion are occupied by Ca^{2+}; another in which two of the neighboring sites contain Ca^{2+} and two are vacant; and a third in which all four sites are vacant. As noted above, none of the model spectra matched the measured spectra well, but they found better agreement with the models that included vacancies. Although the vacancy substitution they consider is the one written by Quartieri et al. (1999a, p. 255, Eq. (c)) as "$^{VIII}[Yb^{3+}] + {}^{VIII}\square = {}^{VIII}[Ca^{2+}/Mg^{2+}] + {}^{IV}[Si^{4+}]$", which is evidently erroneous, it is clear from context that they are concerned with vacancies at the dodecahedral sites, although the specific configuration of Y atoms and vacancies they envision is unclear. The calculations presented here suggest that none of their three modeled configurations would match the lowest-energy—and thus most probable—configuration: in that preferred arrangement, each Yb atom would be surrounded by three Ca^{2+} and one neighboring vacancy (Fig. 1). Quartieri et al. do not present their spectra for pyrope, but in that experimental system the MNZ-MG substitution might also operate, so still different and more complex spectra might be expected.

Energetically favorable substitution schemes: ^{VIII}ALKALI and MNZ. Defects based on the ^{VIII}ALKALI and MNZ substitution schemes are seen in Figure 2 to allow Y+REE incorporation at relatively low energetic cost. These schemes are also the ones for which the strongest evidence exists in nature. As reviewed above, the analytical studies of Enami et al. (1995) on ^{VIII}NA and of Grew et al. (2010) on MNZ-MG and MNZ-FE appear to be definitive confirmations of the importance of those substitution schemes. The predominance of these substitutions in nature is also consistent with inferences from two recent diffusion studies on natural garnet, one in which the menzerite substitution was invoked to explain the linkage of Y+REE diffusivities to the

Always consult and cite the final, published document. See http://www.minsocam.org or GeoscienceWorld

543 mobility of ^{VI}Al (Carlson 2012), and another in which the diffusivity of Li was found to be
544 coupled to the diffusivity of Y+REEs (Cahalan et al. 2012, in review).

545 The study of Grew et al. (2010) is particularly noteworthy for its comprehensiveness in
546 characterizing the crystal chemistry of both the new menzerite-(Y) species and also the Y+REE-
547 rich almandine that occurs in close association. For those crystals, in which alkali components
548 are negligible, their Tables 8 and 9 present calculated compositions in terms of end-members for
549 both garnet species. In menzerite-(Y), the proportion of Y+REE allocated to the menzerite
550 components is 86% on average, whereas on average the yttrogarnet (YAG) component accounts
551 for only 14% of the Y+REE content. Likewise, in their analyses of euhedral almandine—
552 probably the best-characterized and best-equilibrated textural type among their almandine
553 measurements—the proportion of Y+REE allocated to the menzerite components is 90% on
554 average, whereas on average the yttrogarnet (YAG) component accounts for only 10% of the
555 Y+REE content.

556 **Summary.** Taken together, the evidence above presents a consistent picture of the relative
557 importance in nature of the various substitutional schemes we have considered. Atomistic
558 simulation, analytical assessments, and clues from diffusional behavior all point to the
559 dominance of the MNZ-MG and MNZ-FE substitution schemes as the principal means of Y+REE
560 incorporation in garnet, together with the ^{VIII}ALKALI substitution schemes to account for
561 appreciable Na and for small amounts of Li that may be present. The YAG substitution scheme
562 plays only a subordinate role, and the ^{VIII}□ substitution appears to be negligible in nature.

563 **Effects of garnet composition**

564 The results in Figure 2 all show the expected general relationship between exchange energy
565 and garnet composition, in that the energetic cost of all defects is lower in expanded, more

Always consult and cite the final, published document. See http://www.minsocam.org or GeoscienceWorld

566 compliant structures. There are, however, two different types of behavior: those substitutional
567 schemes that replace octahedral Al with a larger ion (MNZ-MG, MNZ-FE, and ^{VI}LI) are much more
568 sensitive to reductions in unit-cell dimension, and thus become substantially higher in energy in
569 contracted structures. As a result, in the pyrope end-member, the ^{VIII}ALKALI substitution schemes
570 are comparable in energy to the MNZ schemes, whereas menzerite components are strongly
571 favored in more expanded structures. This is in accord with the observation of Grew et al. (2010,
572 p. 1183) that the natural menzerite-(Y) garnet in granulites of Parry Sound, Ontario is a solution
573 consisting largely of the end-members $Y_2CaMg_2Si_3O_{12}$ and $Y_2CaFe_2Si_3O_{12}$; that is, the "M" ion
574 associated with the Y+REE component in these garnets is dominantly Ca.

575 All simulations reported here involve only end-member garnet compositions, so we have
576 not considered the possible effects of solid solutions in nature. As van Westrenen et al. (2003)
577 and Freeman et al. (2006) have demonstrated, intermediate compositions within the highly non-
578 ideal pyrope-grossular solid solution may incorporate foreign cations more readily than will
579 either end-member, because doing so can reduce unfavorable interactions between pairs of
580 undersize Mg ions occupying dodecahedra linked by a common Si tetrahedron. This is a
581 substantial effect at low temperatures, but the energetic costs of these unfavorable interactions
582 decrease as temperature rises. Some disparity exists in the literature concerning the temperature
583 at which these interactions become negligible: although the classical calculations of Lavrentiev
584 et al. (2006, p. 343) imply significant avoidance of Mg-Si-Mg groups even at 2000 K, the first-
585 principles calculations of Freeman et al. (2006, p. 6) indicate complete randomization of
586 dodecahedral cations at temperatures in excess of 1000 K. A very different situation exists for
587 the near-ideal pyrope-almandine solid solution, in which the energetic costs of these interactions
588 are greatly reduced at all temperatures, so the effects on trace-element incorporation are

Always consult and cite the final, published document. See http://www.minsocam.org or GeoscienceWorld

589 correspondingly much smaller. For this solid solution, even at low temperature, the fraction of
590 Mg-Si-Mg groups is calculated to be very close to the fraction in a completely random
591 arrangement (Lavrentiev et al. 2006, p. 343), implying a negligible energetic penalty for such
592 interactions. Consequently, we expect that in typical natural occurrences such short-range
593 ordering will be at most a second-order effect, owing to the dominance of garnet compositions
594 comprised principally of pyrope and almandine components, and considering the high
595 temperatures at which garnet crystallizes and equilibrates with coexisting minerals. Nonetheless,
596 it is clear that in solid solutions the energetics may not be a simple combination of end-member
597 results nor a direct function of unit-cell dimension, so additional calculations to quantify the
598 magnitude of solid-solution effects on Y+REE incorporation are needed to strengthen the link
599 between the present end-member results and natural quaternary compositions.

600 A final compositional consideration is the possibility that different substitution schemes
601 operate at different levels of impurity concentration. In olivine, for example, the experimental
602 study of Grant and Wood (2010) concludes that associated neutral LiSc complexes are the
603 dominant means of Li incorporation at concentrations above ~500 ppm Sc, whereas at lower
604 concentrations, this ion pair is dissociated and Li is also incorporated by a scheme involving one
605 Li ion substituting for Mg in an octahedral site, plus one interstitial Li ion. Against that
606 backdrop, it is noteworthy that the substitution schemes identified in this study as low-energy in
607 the dilute limit (M_{NZ} and ^{VIII}ALKALI) are the same as those identified as dominant at very high
608 concentrations by analytical measurements (Enami et al. 1995; Grew et al. 2010). The
609 implication is that trace-element concentration has little effect on the relative energetic costs of
610 potential substitution schemes for Y+REEs in garnet.

611 **Effects of temperature and pressure**

Always consult and cite the final, published document. See http://www.minsocam.org or GeoscienceWorld

From the small variations seen in Figures 3 and 4, one can infer that changes with temperature and pressure in the relative importance of substitutional schemes—for example, the increase in the ^{VIII}NA substitution with pressure reported by Enami et al. (1995) and Røhr et al. (2007)—stem principally from factors other than the defect energies themselves. Two factors are likely to be most significant: (1) the relative energetics of garnet substituents in the phases making up the associated mineral assemblage (e.g., the tendency for Na to be redistributed from plagioclase into minerals of smaller molar volume, including garnet, with increasing pressure); and (2) the dependence of garnet composition on temperature and pressure (e.g., the relative stability of pyropic components at higher pressure, with its concomitant tendency to destabilize the MNZ-MG and MNZ-FE substitutions relative to the ^{VIII}NA substitution).

Effects of ionic radius for REEs

Because REEs substitute for smaller ions in the dodecahedral sites of garnet, higher exchange energies are expected for ions with larger radii, and this effect is seen in Table 7 and Figure 5 to be very large. The contraction of ionic radii with increasing atomic number across the lanthanides thus results in a substantial lowering of the defect and exchange energies, which is consistent with—and of course is the underlying explanation for—the strong preference of garnet for HREEs over LREEs, as expressed in garnet-melt partition coefficients (cf. van Westrenen et al. 2000) and in partitioning between garnet and diverse minerals in common metamorphic assemblages (e.g., Gieré et al. 2011, among many others).

The substitutional schemes with the highest exchange energies are also those with the greatest dependence on ionic radius (i.e., with the steepest slopes and strongest curvature in Fig. 5). This implies that the dominant cause of the elevated exchange energies for those schemes is

Always consult and cite the final, published document. See http://www.minsocam.org or GeoscienceWorld

634 the strain associated with accommodation of the oversize Y+REE ion; the alternative, lower-
635 energy schemes are evidently better able to compensate for this strain.

636 **Defect association and migration at elevated temperatures**

637 Two generalities emerge from the comparison in Appendix 1 (Depository item AM-
638 YEAR-XXX) of free energies at 1200 K and 2 GPa for differently-configured defects. First, the
639 free energies at 1200 K of dissociated defects (in which the charge-compensating ions are
640 separated by a distance sufficient to produce only negligible interactions between them) are in
641 general ~200 $kJ \cdot mol^{-1}$ higher than the free energies of the associated defects in all configurations.
642 This indicates that these defects will tend to remain strongly associated—producing local charge
643 compensation—even at high temperature. Second, the minimum-energy configurations are lower
644 in energy by about 10-30 $kJ \cdot mol^{-1}$ in comparison to alternative arrangements for which the
645 charge-compensating ions are progressively more distant from one another. At 1200 K, the
646 quantity RT has the value 10 $kJ \cdot mol^{-1}$, so under geologic conditions appreciable fractions of the
647 defects could adopt those higher-energy alternative configurations. Transient occupancy of such
648 higher-energy states is required for associated defects to migrate via diffusion, so both results are
649 consistent with, and provide explanations for, the observed coupled movement of charge-
650 compensating groups during diffusional transport of Y+REEs (cf. Carlson 2012; Cahalan et al. in
651 review).

652 **IMPLICATIONS**

653 The results of this study should strongly discourage the long-standing practice of assuming,
654 without direct evidence, that the YAG substitution accounts for Y+REE contents in garnet when
655 Na does not provide charge-balance. Because the YAG substitution is energetically strongly
656 disfavored, uncritical acceptance of YAG components as a prominent form of Y+REE

Always consult and cite the final, published document. See http://www.minsocam.org or GeoscienceWorld

657 incorporation in natural garnet is not warranted. Furthermore, because the $^{VIII}\square$ substitution is so
658 energetically costly that it is likely to be almost entirely inoperative, explanations for natural
659 Y+REE incorporation should be sought first in terms of the MNZ-MG, MNZ-FE, and ^{VIII}NA
660 substitutions. One example of the implications of this recognition is that recasting the
661 thermodynamic properties of Y+REE in garnet in terms of these non-YAG components may
662 simplify key relationships between garnet and mantle-sourced melts, and between garnet and the
663 various Y+REE-rich accessory minerals whose evolution it tracks.

664 Although this work was focused on Y+REEs, and consequently did not undertake a
665 comprehensive investigation of modes of incorporation of Na and Li, it nevertheless has
666 implications for alkali components in garnet. The demonstration that the substitution coupling
667 Y^{3+} with Na^{+} in dodecahedral sites is an energetically favorable option for Y+REE uptake
668 confirms prior analytical recognition of that substitution as the dominant means of Na
669 incorporation. Although the analogous substitution involving $^{VIII}Li^{+}$ will ordinarily have little
670 impact on total Y+REE concentration, it is evidently the principal avenue for Li incorporation
671 into garnet, and the consequent diffusional coupling of Li with Y+REEs holds out promise that
672 retentivity of Li zoning in garnet is high, which should make garnet a uniquely robust monitor of
673 Li systematics in high-grade metamorphic rocks.

674 By providing corroborative evidence substantiating the inference of Carlson (2012) that
675 diffusion of Y+REEs in garnet may proceed predominantly by means of exchanges based on the
676 MNZ-MG and MNZ-FE substitutions, this work greatly improves prospects for systematizing their
677 diffusional behavior. Although investigation of the kinetics of diffusion mechanisms that link
678 Y+REE mobility to Na transport is still needed, the present results severely diminish the
679 likelihood that multiple diffusion mechanisms, each with distinctly different kinetics, might

Always consult and cite the final, published document. See http://www.minsocam.org or GeoscienceWorld

contribute to Y+REE transport in garnet, or that different mechanisms may predominate in different thermal or barometric regimes.

Finally, the present findings should provide guidance for future experimental and analytical studies. They establish a set of testable hypotheses concerning the relative importance of diverse substitutional schemes; they predict the defect configurations that are most likely to be encountered in future structural studies (e.g., in XAFS measurements and modeling); and they identify the transport mechanisms that must be activated in future diffusional measurements for those experiments to be fully relevant to natural systems.

ACKNOWLEDGEMENTS

This work was funded by U.S. National Science Foundation Grant EAR-1144309 to WDC, and by support from the Australian Research Council to JDG/KW. WDC gratefully acknowledges the generous aid and assistance of numerous colleagues at Curtin University's Department of Chemistry and Nanochemistry Research Institute during a collaborative research visit there, made possible by a Faculty Development Grant from the University of Texas, and by funding from the University's Jackson School of Geological Sciences. We thank Wim van Westrenen for a valuable review that helped in many ways to clarify the presentation and that brought to our attention the potential importance of solid-solution effects.

REFERENCES CITED

Allan, N.L., Barron, T.H.K., and Bruno, J.A.O. (1996) The zero static internal stress approximation in lattice dynamics, and the calculation of isotope effects on molar volumes. Journal of Chemical Physics, 105, 8300-8303.

Always consult and cite the final, published document. See http://www.minsocam.org or GeoscienceWorld

Babuška, V., Fiala, J., Kumazawa, M., and Ohno, I. (1978) Elastic properites of garnet solid-solution series. Physics of the Earth and Planetary Interiors, 16, 157-176.

Bea, F., Montero, P., Garuti, G., and Zacharini, F. (1997) Pressure-dependence of rare earth element distribution in amphibolite- and granulite-grade garnets. A LA-ICP-MS study. Geostandards Newsletter, 21, 253-270.

Becker, U., and Pollok, K. (2002) Molecular simulations of interfacial and thermodynamic mixing properties of grossular-andradite garnets. Physics and Chemistry of Minerals, 29, 52-64.

Bosenick, A., Dove, M.T., and Geiger, C.A. (2000) Simulation studies on the pyrope-grossular garnet solid solution. Physics and Chemistry of Minerals, 27, 398-418.

Cahalan, R.C., Kelly, E.D., and Carlson, W.D. (2012) Coupled diffusion of lithium and yttrium (+HREE) in garnet. Abstract V23D-2856, 2012 Fall Meeting, American Geophysical Union, San Francisco CA.

_____. (in review) Rates of Li diffusion in garnet: Coupled diffusion of Li and Y+REEs. Submitted July 2013 to American Mineralogist.

Carlson, W.D. (2012) Rates and mechanism of Y, REE, and Cr diffusion in garnet. American Mineralogist, 97, 1598-1618.

Dick, B.G., Jr., and Overhauser, A.W. (1958) Theory of the dielectric constants of alkali halide crystals. Physical Review, 112, 90-103.

Enami, M., Cong, B., Yoshida, H., and Kawabe, I. (1995) A mechanism for Na incorporation in garnet: An example from garnet in orthogneiss from the Su-Lu terrane, eastern China. American Mineralogist, 80, 475-482.

Always consult and cite the final, published document. See http://www.minsocam.org or GeoscienceWorld

Farley, T.W.D., Hayes, W., Hull, S., Ward, R., Hutchings, M.T., and Alba, M. (1988) The dynamic properties of lithium oxide investigated by neutron scattering techniques. Solid State Ionics, 28-30, 189-193.

Freeman, C.L., Allan, N.L., and van Westrenen, W. (2006) Local cation environments in the pyrope-grossular $Mg_3Al_2Si_3O_{12}$–$Ca_3Al_2Si_3O_{12}$ garnet solid solution. Physical Review B, 74:134203.

Freeman, C.L., Lavrentiev, M.Y., Allan, N.L., Purton, J.A., and van Westrenen, W. (2005) Similarity in silicate chemistry: Trace elements in garnet solid solutions. Journal of Molecular Structure: THEOCHEM, 727, 199-204.

Gale, J.D. (1997) GULP: A computer program for the symmetry-adapted simulation of solids. Faraday Transactions, 93, 629-637.

_____. (1998) Analytical free energy minimization of silica polymorphs. Journal of Physical Chemistry B, 102, 5423-5431.

Gale, J.D., and Rohl, A.L. (2003) The General Utility Lattice Program (GULP). Molecular Simulation, 29, 291-341.

Ganguly, J., Cheng, W., and O'Neill, H.S.C. (1993) Syntheses, volume, and structural changes of garnets in the pyrope-grossular join: Implications for stability and mixing properties. American Mineralogist, 78, 583-593.

Geiger, C.A., and Feenstra, A. (1997) Molar volumes of mixing of almandine-pyrope and almandine-spessartine garnets and the crystal chemistry and thermodynamic-mixing properties of the aluminosilicate garnets. American Mineralogist, 82, 571-581.

Always consult and cite the final, published document. See http://www.minsocam.org or GeoscienceWorld

Gieré, R., Rumble, D., Günther, D., Connolly, J., and Caddick, M.J. (2011) Correlation of growth and breakdown of major and accessory minerals in metapelites from Campolungo, central Alps. Journal of Petrology, 52, 2293-2334.

Grant, K.J., and Wood, B.J. (2010) Experimental study of the incorporation of Li, Sc, Al and other trace elements into olivine. Geochimica et Cosmochimica Acta, 74, 2412-2428.

Grew, E.S., Marsh, J.H., Yates, M.G., Lazic, B., Armbruster, T., Locock, A., Bell, S.W., Dyar, M.D., Bernhardt, H.-J., and Medenbach, O. (2010) Menzerite-(Y), a new species, $\{(Y, REE)(Ca, Fe^{2+})_2\}[(Mg, Fe^{2+})(Fe^{3+}, Al)](Si_3)O_{12}$, from a felsic granulite, Parry Sound, Ontario, and a new garnet end-member, $\{Y_2Ca\}[Mg_2](Si_3)O_{12}$. Canadian Mineralogist, 48, 1171-1193.

Hanrahan, M., Brey, G., Woodland, A., Seitz, H.-M., and Ludwig, T. (2009) Li as a barometer for bimineralic eclogites: Experiments in natural systems. Lithos, 112S, 992-1001.

Hanson, G.N. (1980) Rare earth elements in petrogenetic studies of igneous systems. Annual Review of Earth and Planetary Science, 8, 371-406.

Hermann, J., and Rubatto, D. (2003) Relating zircon and monazite domains to garnet growth zones: Age and duration of granulite-facies metamorphism in the Val Malenco lower crust. Journal of Metamorphic Geology, 21, 833-852.

Jaffe, H.W. (1951) The role of yttrium and other minor elements in the garnet group. American Mineralogist, 36, 133-155.

Kantorovich, L.N. (1995) Thermoelastic properties of perfect crystals with nonprimitive lattices. I. General theory. Physical Review B, 51, 3520-3534.

Kasowski, M.A., and Hogarth, D.D. (1968) Yttrian andradite from the Gatineau Park, Quebec. Canadian Mineralogist, 9, 552-558.

Always consult and cite the final, published document. See http://www.minsocam.org or GeoscienceWorld

768 Kelly, E.D., Carlson, W.D., and Connelly, J.N. (2011) Implications of garnet resorption for the
769 Lu-Hf garnet geochronometer: An example from the contact aureole of the Makhavinekh
770 Lake Pluton, Labrador. Journal of Metamorphic Geology, 29, 901-916.
771 Kohn, M.J. (2009) Models of garnet differential chronology. Geochimica et Cosmochimica Acta,
772 73, 170-182.
773 Konrad-Schmolke, M., Zack, T., O'Brien, P.J., and Jacob, D.E. (2008) Combined
774 thermodynamic and rare earth element modelling of garnet growth during subduction:
775 Examples from ultrahigh-pressure eclogite of the Western Gneiss Region, Norway. Earth
776 and Planetary Science Letters, 272, 488-498.
777 Lavrentiev, M.Y., van Westrenen, W., Allan, N.L., Freeman, C.L., and Purton, J.A. (2006)
778 Simulation of thermodynamic mixing properties of garnet solid solutions at high
779 temperatures and pressures. Chemical Geology, 225, 336-346.
780 Lewis, G.V., and Catlow, C.R.A. (1985) Potential models for ionic oxides. Journal of Physics. C,
781 Solid State Physics, 18, 1149-1161.
782 Menzer, G. (1928) Die Kristallstruktur der Granate. Zeitschrift für Kristallographie, 69, 300-396.
783 Moore, S.J., Carlson, W.D., and Hesse, M.A. (2013) Origins of yttrium and rare-earth-element
784 distributions in metamorphic garnet. Journal of Metamorphic Geology, 31, 663-689.
785 Mott, N.F., and Littleton, M.J. (1938) Conduction in polar crystals. I. Electrolytic conduction in
786 solid salts. Transactions of the Faraday Society, 34, 485-499.
787 Purton, J.A., Allan, N.L., and Blundy, J.D. (1997) Calculated solution energies of heterovalent
788 cations in forsterite and diopside: Implications for trace-element partitioning. Geochimica
789 et Cosmochimica Acta, 61, 3927-3936.

Always consult and cite the final, published document. See http://www.minsocam.org or GeoscienceWorld

Purton, J.A., Allan, N.L., Blundy, J.D., and Wasserman, E.A. (1996) Isovalent trace element partitioning between minerals and melts — a computer simulation model. Geochimica et Cosmochimica Acta, 60, 4977-4987.

Pyle, J.M., and Spear, F.S. (1999) Yttrium zoning in garnet: Coupling of major and accessory phases during metamorphic reactions. Geological Materials Research, 1, no. 6.

_____. (2000) An empirical garnet (YAG) - xenotime thermometer. Contributions to Mineralogy and Petrology, 138, 51-58.

Pyle, J.M., Spear, F.S., Rudnick, R.L., and McDonough, W.F. (2001) Monazite-xenotime-garnet equilibrium in metapelites and a new monazite-garnet thermometer. Journal of Petrology, 42, 2083-2107.

Quartieri, S., Antonioli, G., Geiger, C.A., Artioli, G., and Lottici, P.P. (1999a) XAFS characterization of the structural site of Yb in synthetic pyrope and grossular garnets. Physics and Chemistry of Minerals, 26, 251-256.

Quartieri, S., Chaboy, J., Antonioli, G., and Geiger, C.A. (1999b) XAFS characterization of the structural site of Yb in synthetic pyrope and grossular garnets. II. XANES full multiple scattering calculations at the Yb L_I- and L_{III}-edges. Physics and Chemistry of Minerals, 27, 88-94.

Røhr, T., H, A., and Erambert, M. (2007) Stress-induced redistribution of yttrium and heavy rare-earth elements (HREE) in garnet during high-grade polymetamorphism. American Mineralogist, 92, 1276-1287.

Rubatto, D. (2002) Zircon trace element geochemistry: Partitioning with garnet and the link between U-Pb ages and metamorphism. Chemical Geology, 184, 123-138.

Always consult and cite the final, published document. See http://www.minsocam.org or GeoscienceWorld

812 Sanders, M.J., Leslie, M., and Catlow, C.R.A. (1984) Interatomic potentials for SiO_2. Journal of
813 the Chemical Society, Chemical Communications, 1271-1273.
814 Semenov, E.I. (1963) Mineralogy of the Rare Earths. Izdatel'stvo Akademii Nauk SSSR,
815 Moscow, Russia (in Russian).
816 Shannon, R.D. (1976) Revised effective ionic radii and systematic studies of interatomic
817 distances in halides and chalcogenides. Acta Crystallographica, A32, 751-767.
818 Skora, S., Baumgartner, L.P., Mahlen, N.J., Johnson, C.M., Pilet, S., and Hellebrand, E. (2006)
819 Diffusion-limited REE uptake by eclogite garnets and its consequences for Lu–Hf and
820 Sm–Nd geochronology. Contributions to Mineralogy and Petrology, 152, 703-720.
821 Sun, C., and Liang, Y. (2013) The importance of crystal chemistry on REE partitioning between
822 mantle minerals (garnet, clinopyroxene, orthopyroxene, and olivine) and basaltic melts.
823 Chemical Geology, 358, 23-36.
824 Taylor, M.B., Barrera, G.D., Allan, N.L., Barron, T.H.K., and Mackrodt, W.C. (1997) Free
825 energy of formation of defects in polar solids. Faraday Discussions, 106, 377-387.
826 Tirone, M., Ganguly, J., Dohmen, R., Langenhorst, F., Hervig, R., and Becker, H.-W. (2005)
827 Rare earth diffusion kinetics in garnet: Experimental studies and applications.
828 Geochimica et Cosmochimica Acta, 69, 2385-2398.
829 Van Orman, J.A., Grove, T.L., Shimizu, N., and Layne, G.D. (2002) Rare earth element
830 diffusion in a natural pyrope single crystal at 2.8 GPa. Contributions to Mineralogy and
831 Petrology, 142, 416-424.
832 van Westrenen, W., Allan, N.L., Blundy, J.D., Lavrentiev, M.Y., Lucas, B.R., and Purton, J.A.
833 (2003a) Dopant incorporation into garnet solid solutions – a breakdown of Goldschmidt's
834 first rule. Chemical Communications, 786-787.

Always consult and cite the final, published document. See http://www.minsocam.org or GeoscienceWorld

_____. (2003b) Trace element incorporation into pyrope-grossular solid solutions: An atomistic simulation study. Physics and Chemistry of Minerals, 30, 217-229.

van Westrenen, W., Allan, N.L., Blundy, J.D., Purton, J.A., and Wood, B.J. (2000) Atomistic simulation of trace element incorporation into garnets — comparison with experimental garnet-melt partitioning data. Geochimica et Cosmochimica Acta, 64, 1629-1639.

van Westrenen, W., and Draper, D.S. (2007) Quantifying garnet-melt trace element partitioning using lattice strain theory: new crystal-chemical and thermodynamic constraints. Contributions to Mineralogy and Petrology, 154, 717-730.

Vinograd, V.L., Sluiter, M.H.F., Winkler, B., Putnis, A., Hålenius, U., Gale, J.D., and Becker, U. (2004) Thermodynamics of mixing and ordering in pyrope-grossular solid solution. Mineralogical Magazine, 68, 101-121.

Vinograd, V.L., Winkler, B., Putnis, A., Kroll, H., Milman, V., Gale, J.D., and Fabrichnaya, O.B. (2006) Thermodynamics of pyrope-majorite, $Mg_3Al_2Si_3O_{12}$–$Mg_4Si_4O_{12}$, solid solution from atomistic model calculations. Molecular Simulation, 32, 85-99.

Yang, P., and Pattison, D.R.M. (2006) Genesis of monazite and yttrium zoning in garnet from the Black Hills, South Dakota. Lithos, 88, 233-253.

Yang, P., and Rivers, T. (2002) The origin of Mn and Y annuli in garnet and the thermal dependence of P in garnet and Y in apatite in calc-pelite and pelite, Gagnon terrane, western Labrador. Geological Materials Research, 4, 1-35.

Yoder, H.S., and Keith, M.L. (1951) Complete substitution of aluminum for silicon: The system $3MnO{\cdot}Al_2O_3{\cdot}3SiO_2 – 3Y_2O_3{\cdot}5Al_2O_3$. American Mineralogist, 36, 519-533.

Always consult and cite the final, published document. See http://www.minsocam.org or GeoscienceWorld

FIGURE CAPTIONS

FIGURE 1. Portions of garnet structure illustrating minimum-energy configurations for Y incorporation by means of different charge-compensating substitution schemes. In the unmodified structure, red tetrahedra are occupied by Si; blue octahedra are occupied by Al; and yellow dodecahedra are occupied by divalent cations Mg, Fe, Mn, and Ca. Labels on polyhedra indicate occupancy for substitution schemes (in boxes) described in text; "□" indicates a vacant (unoccupied) dodecahedron. Structures are redrawn with modification from Bosenick et al. (2000) Figs. 1 (*left*) and 4 (*right*).

FIGURE 2. Exchange free energies ΔG_{xch} for Y incorporation into end-member Pyp, Alm, Sps, and Grs at 1200 K and 2 GPa, referenced to binary oxides as sources and sinks for exchanged cations.

FIGURE 3. Defect free energies ΔG_{def} for Y incorporation into almandine as functions of temperature, at 2 GPa. Vertical scaling is the same for all diagrams, and spans only 50 $kJ \cdot mol^{-1}$.

FIGURE 4. Defect free energies ΔG_{def} for Y incorporation into almandine as functions of pressure, at 1200 K. Vertical scaling is the same for all diagrams, and spans only 50 $kJ \cdot mol^{-1}$.

FIGURE 5. Exchange free energies ΔG_{xch} for incorporation of selected REEs into almandine at 1200 K and 2 GPa, referenced to binary oxides as sources and sinks for exchanged cations.

Always consult and cite the final, published document. See http://www.minsocam.org or GeoscienceWorld

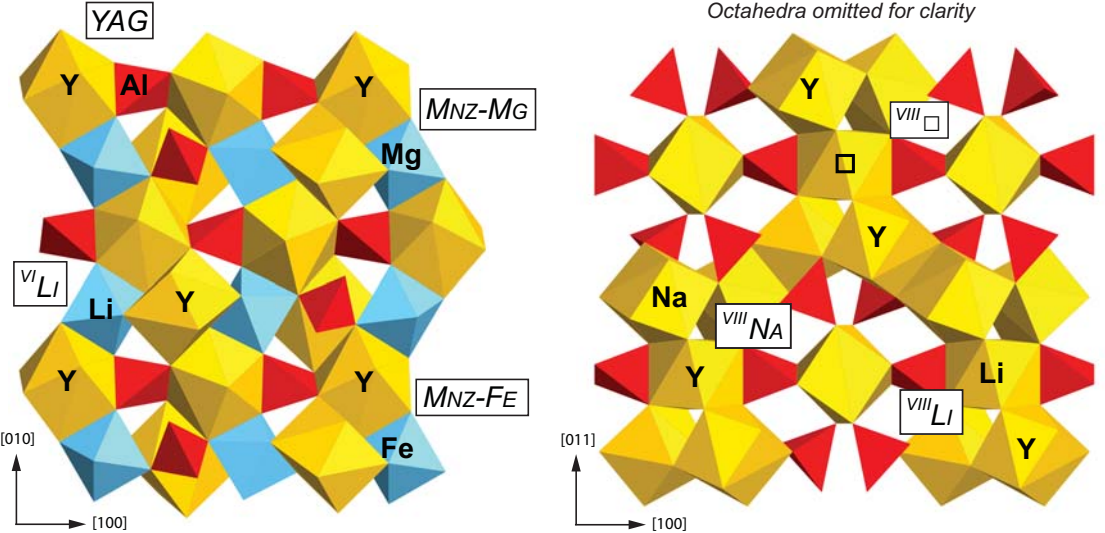

4720-R1 Carlson et al. FIGURE 1

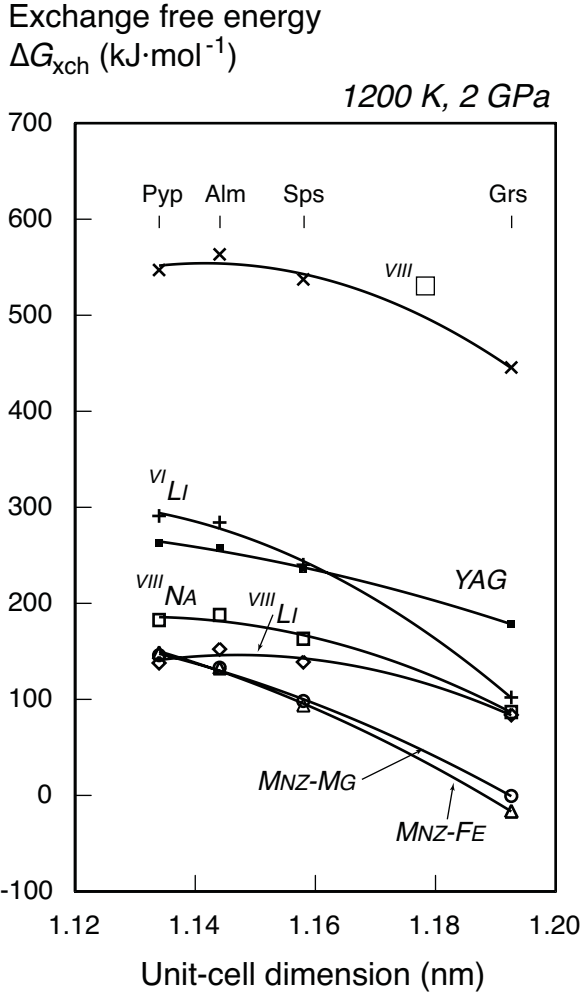

4720-R1 Carlson et al. FIGURE 2

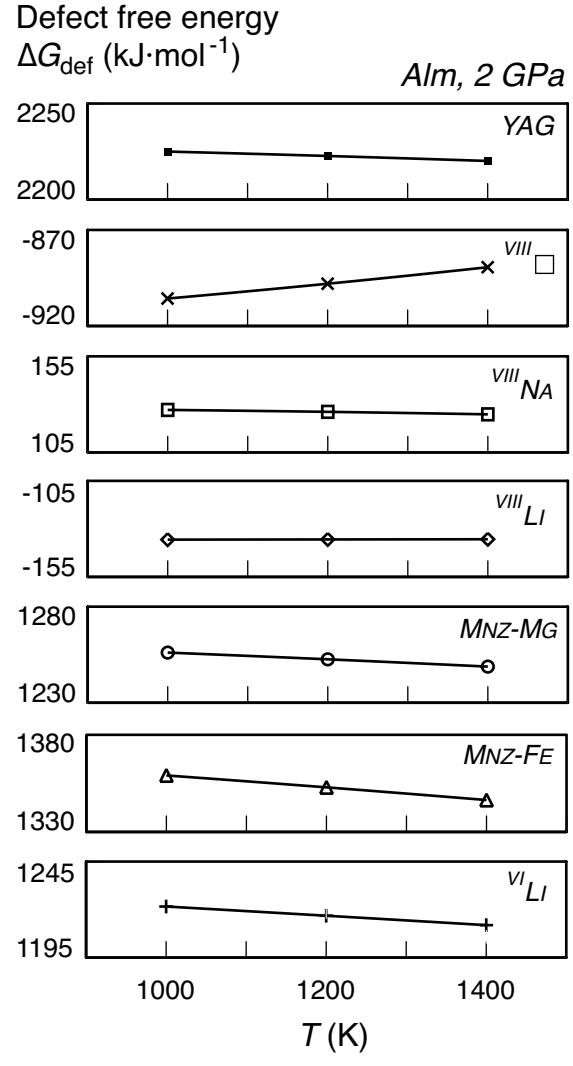

4720-R1 Carlson et al. FIGURE 3

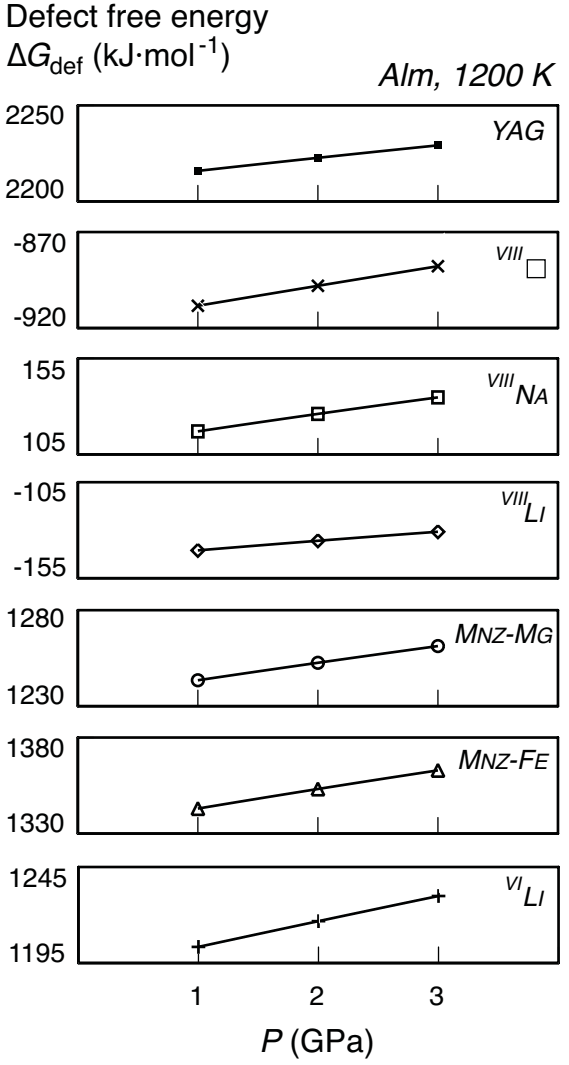

4720-R1 Carlson et al. FIGURE 4

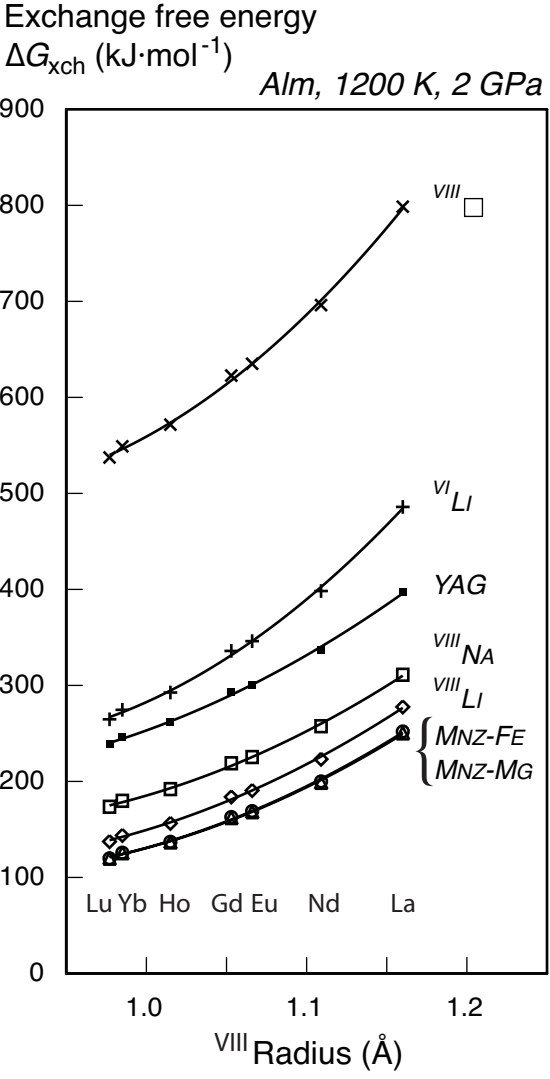

4720-R1 Carlson et al. FIGURE 5

TABLE 1. Parameters for interatomic potentials

Interaction	A (kJ·mol^{-1})	ρ (Å)	C (kJ·mol^{-1}·Å^6)	Source
$Li^+ – O^{2-}$	69788.4	0.2863	0	5
$Na^+ – O^{2-}$	122231.1	0.3065	0	4
$Mg^{2+} – O^{2-}$	137829	0.2945	0	3
$Al^{3+} – O^{2-}$	107571.5	0.3118	0	2
$Si^{4+} – O^{2-}$	123878	0.3205	1028	1
$Ca^{2+} – O^{2-}$	105207	0.3437	0	3
$Mn^{2+} – O^{2-}$	97199	0.3262	0	3
$Fe^{2+} – O^{2-}$	116515	0.3084	0	3
$Y^{3+} – O^{2-}$	129782.4	0.3491	0	2
$La^{3+} – O^{2-}$	138909.5	0.3651	0	2
$Nd^{3+} – O^{2-}$	133139.7	0.3601	0	2
$Eu^{3+} – O^{2-}$	131026.6	0.3556	0	2
$Gd^{3+} – O^{2-}$	128981.1	0.3551	0	2
$Ho^{3+} – O^{2-}$	130274.0	0.3487	0	2
$Yb^{3+} – O^{2-}$	126356.8	0.3462	0	2
$Lu^{3+} – O^{2-}$	129974.9	0.3430	0	2
$O^{2-} – O^{2-}$	2196384	0.1490	2690	1

Interaction	shell charge (|e|)	k (kJ·mol^{-1}·Å^{-2})	Source
O^{2-} (core-shell)	-2.86902	7229	3, 1

Interaction	K_B (kJ·mol^{-1}·rad^{-2})	θ_0 (°)	Source
$O^{2-} – Si^{4+} – O^{2-}$	2.097	109.47	1

Notes: Sources: 1 = Sanders et al. (1984); 2 = Lewis and Catlow (1985); 3 = Purton et al. (1996); 4= Purton et al. (1997); 5 = this study. All short-range interactions for O^{2-} act on the shell of the ion. The cut-off distance for the metal-oxygen Buckingham potentials was 12 Å.

TABLE 2. Experimental and calculated unit-cell dimensions a_0 (nm), bulk moduli κ (GPa), and shear moduli μ_V (GPa)

	Experimental	Potential Set 1	Potential Set 2
a_0 (Pyp)	1.1457	1.1310	1.1274
a_0 (Alm)	1.1525	1.1414	1.1496
a_0 (Sps)	1.1614	1.1557	1.1663
a_0 (Grs)	1.1852	1.1903	1.1777
κ (Pyp)	173.0	209.3	212.3
κ (Alm)	177.9	204.3	196.8
κ (Sps)	174.2	197.9	194.2
κ (Grs)	169.1	189.0	208.9
μ_V (Pyp)	92.1	117.0	129.6
μ_V (Alm)	96.7	114.5	120.9
μ_V (Sps)	94.8	110.5	119.8
μ_V (Grs)	105.3	100.5	126.8

Notes: Observations and calculations for T = 298 K, P = 0.0001 GPa. Potential Set 1 = this study; Potential Set 2 = Bosenick et al. (2000). Unit-cell dimensions from Ganguly et al. (1993) and Geiger and Feenstra (1997). Experimental bulk moduli and shear moduli (Voight convention) from Babuška et al. (1978).

TABLE 3. Substitutional exchange reactions

Substitution scheme	Exchange vector	Reaction
YAG	$[YM_{-1}\cdot AlSi_{-1}]$	$M_3Al_2Si_3O_{12} + ½\ Y_2O_3 + ½\ Al_2O_3 = YM_2\cdot Al_2\cdot AlSi_2\cdot O_{12} + MO + SiO_2$
$^{VIII}\square$	$[Y_2\square M_{-3}]$	$M_3Al_2Si_3O_{12} + Y_2O_3 = Y_2\square\cdot Al_2\cdot Si_3\cdot O_{12} + 3\ MO$
^{VIII}NA	$[YNaM_{-2}]$	$M_3Al_2Si_3O_{12} + ½\ Y_2O_3 + ½\ Na_2O = YNaM\cdot Al_2\cdot Si_3\cdot O_{12} + 2\ MO$
^{VIII}LI	$[YLiM_{-2}]$	$M_3Al_2Si_3O_{12} + ½\ Y_2O_3 + ½\ Li_2O = YLiM\cdot Al_2\cdot Si_3\cdot O_{12} + 2\ MO$
MNZ-MG	$[YM_{-1}\cdot MgAl_{-1}]$	$M_3Al_2Si_3O_{12} + ½\ Y_2O_3 + MgO = YM_2\cdot MgAl\cdot Si_3\cdot O_{12} + MO + ½\ Al_2O_3$
MNZ-FE	$[YM_{-1}\cdot FeAl_{-1}]$	$M_3Al_2Si_3O_{12} + ½\ Y_2O_3 + FeO = YM_2\cdot FeAl\cdot Si_3\cdot O_{12} + MO + ½\ Al_2O_3$
^{VI}LI	$[Y_2M_{-2}\cdot LiAl_{-1}]$	$M_3Al_2Si_3O_{12} + Y_2O_3 + ½\ Li_2O = Y_2M\cdot LiAl\cdot Si_3\cdot O_{12} + 2\ MO + ½\ Al_2O_3$

Notes: "M" = Mg, Fe, Mn, or Ca; □ = dodecahedral vacancy.

TABLE 4. Lattice free energies (in kJ·mol^{-1}) for binary oxides

T (K)	1000	1000	1000	1200	1200	1200	1400	1400	1400
P (GPa)	1	2	3	1	2	3	1	2	3
Li_2O	-3017	-3001	-2985	-3041	-2998	-2982	-3031	-3015	-2999
Na_2O	-2585	-2557	-2531	-2618	-2546	-2519	-2595	-2568	-2541
MgO	-4000	-3990	-3978	-4018	-3985	-3973	-4005	-3994	-3983
Al_2O_3	-15560	-15536	-15512	-15599	-15553	-15529	-15615	-15590	-15566
SiO_2	-12431	-12410	-12389	-12455	-12415	-12394	-12458	-12436	-12415
CaO	-3495	-3477	-3461	-3515	-3467	-3450	-3496	-3478	-3461
MnO	-3773	-3759	-3746	-3792	-3747	-3734	-3773	-3759	-3746
FeO	-3907	-3895	-3883	-3926	-3884	-3872	-3907	-3894	-3882
Y_2O_3	-13119	-13067	-13024	-13157	-13113	-13069	-13207	-13163	-13118
La_2O_3					-12290				
Nd_2O_3					-12595				
Eu_2O_3					-12827				
Gd_2O_3					-12888				
Ho_2O_3					-13150				
Yb_2O_3					-13343				
Lu_2O_3					-13423				

TABLE 5. Defect free energies ΔG_{def} (in kJ·mol^{-1}) for Y incorporation into garnet

Host	T (K)	P (GPa)	YAG	$^{VIII}\square$	^{VIII}NA	^{VIII}LI	MNZ-MG	MNZ-FE	^{VI}LI
Pyp	1000	1	2326	-625	318	50	1363	1469	1421
Pyp	1000	2	2334	-611	329	57	1373	1480	1436
Pyp	1000	3	2342	-598	340	64	1383	1490	1451
Pyp	1200	1	2321	-625	312	45	1356	1459	1410
Pyp	1200	2	2329	-611	323	52	1366	1470	1426
Pyp	1200	3	2337	-598	334	59	1376	1481	1441
Pyp	1400	1	2315	-625	305	40	1349	1449	1400
Pyp	1400	2	2323	-611	316	47	1360	1460	1415
Pyp	1400	3	2331	-598	327	54	1370	1471	1430
Alm	1000	1	2219	-916	119	-140	1248	1350	1209
Alm	1000	2	2225	-906	127	-136	1256	1359	1222
Alm	1000	3	2232	-895	136	-130	1265	1370	1235
Alm	1200	1	2216	-908	117	-140	1243	1343	1203
Alm	1200	2	2223	-898	126	-135	1253	1353	1217
Alm	1200	3	2229	-888	135	-131	1261	1363	1230
Alm	1400	1	2213	-900	115	-141	1239	1336	1198
Alm	1400	2	2220	-889	125	-135	1249	1347	1212
Alm	1400	3	2227	-880	133	-131	1258	1356	1225
Sps	1000	1	2061	-1348	-177	-424	1077	1175	894
Sps	1000	2	2067	-1341	-170	-421	1085	1184	905
Sps	1000	3	2072	-1335	-165	-419	1093	1193	916
Sps	1200	1	2059	-1338	-177	-423	1074	1169	890
Sps	1200	2	2064	-1332	-171	-421	1082	1178	901
Sps	1200	3	2070	-1326	-165	-419	1089	1187	911
Sps	1400	1	2057	-1328	-177	-423	1071	1163	885
Sps	1400	2	2062	-1323	-171	-421	1078	1172	896
Sps	1400	3	2067	-1317	-165	-419	1086	1181	907
Grs	1000	1	1728	-2270	-806	-1032	701	788	202
Grs	1000	2	1729	-2274	-808	-1037	705	793	207
Grs	1000	3	1730	-2279	-809	-1042	710	799	212
Grs	1200	1	1725	-2262	-807	-1032	697	781	196
Grs	1200	2	1727	-2266	-809	-1038	702	787	201
Grs	1200	3	1728	-2271	-810	-1043	706	793	206
Grs	1400	1	1723	-2252	-808	-1032	694	775	190
Grs	1400	2	1725	-2257	-810	-1038	698	781	195
Grs	1400	3	1726	-2262	-811	-1043	703	787	200

TABLE 6. Exchange free energies ΔG_{xch} (in kJ·mol^{-1}) for Y incorporation into garnet

Host	T (K)	P (GPa)	YAG	$^{VIII}\square$	^{VIII}NA	^{VIII}LI	MNZ-MG	MNZ-FE	^{VI}LI
Pyp	1000	1	234	493	169	117	143	155	267
Pyp	1000	2	237	489	163	113	139	151	257
Pyp	1000	3	243	492	161	112	139	151	255
Pyp	1200	1	227	480	164	110	135	147	254
Pyp	1200	2	263	547	183	138	146	149	291
Pyp	1200	3	269	551	181	138	146	149	289
Pyp	1400	1	262	566	195	148	145	146	304
Pyp	1400	2	270	570	193	148	146	147	302
Pyp	1400	3	276	573	192	148	146	147	300
Alm	1000	1	220	482	156	113	120	129	242
Alm	1000	2	222	477	149	109	116	125	232
Alm	1000	3	228	480	148	108	116	126	230
Alm	1200	1	212	470	152	106	113	122	229
Alm	1200	2	258	563	188	152	133	133	284
Alm	1200	3	264	566	186	152	133	133	282
Alm	1400	1	259	587	204	165	134	132	300
Alm	1400	2	266	591	202	165	135	133	298
Alm	1400	3	272	593	200	164	134	133	296
Sps	1000	1	197	455	131	100	85	89	197
Sps	1000	2	200	450	125	95	81	86	188
Sps	1000	3	206	453	122	95	81	86	186
Sps	1200	1	190	443	126	92	78	83	184
Sps	1200	2	236	537	163	139	98	94	240
Sps	1200	3	241	540	161	138	98	94	238
Sps	1400	1	237	561	179	151	100	93	255
Sps	1400	2	244	564	177	150	100	94	253
Sps	1400	3	250	566	174	150	100	94	252
Grs	1000	1	141	365	56	47	-14	-20	60
Grs	1000	2	143	360	49	42	-17	-24	51
Grs	1000	3	148	363	47	41	-17	-23	51
Grs	1200	1	133	351	51	38	-21	-28	45
Grs	1200	2	178	446	87	84	-1	-16	102
Grs	1200	3	184	448	84	83	0	-16	101
Grs	1400	1	180	468	102	96	0	-18	114
Grs	1400	2	187	471	100	94	0	-17	113
Grs	1400	3	193	474	97	94	1	-16	113

TABLE 7. Exchange free energies ΔG_{xch} (in kJ·mol^{-1}) for REE incorporation into almandine at 1200 K and 2 GPa

REE	YAG	$^{VIII}\square$	^{VIII}NA	^{VIII}LI	MNZ-MG	MNZ-FE	^{VI}LI
La	397	799	311	278	252	250	486
Nd	337	696	257	223	200	199	398
Eu	301	635	225	191	169	168	346
Gd	293	623	219	184	163	162	336
Ho	262	572	192	156	137	137	293
Yb	246	549	180	144	126	126	275
Lu	239	537	174	137	120	120	265